Letter

Relaxation timescales and electron-phonon coupling in optically pumped $YBa_2Cu_3O_{6+x}$ revealed by time-resolved Raman scattering

N. Pellatz,[1,2] S. Roy,[1,2] J-W. Lee,[3] J. L. Schad,[3] H. Kandel,[4] N. Arndt,[4] C. B. Eom,[3] A. F. Kemper,[5] and D. Reznik[1,2,*]

[1]*Department of Physics, University of Colorado, Boulder, Colorado 80309, USA*

[2]*Center for Experiments on Quantum Materials, University of Colorado, Boulder, Colorado 80309, USA*

[3]*Department of Materials Science and Engineering, University of Wisconsin, Madison, Wisconsin 53706, USA*

[4]*Department of Physics and Mathematics, University of Wisconsin–Parkside, Kenosha, Wisconsin 53140, USA*

[5]*Department of Physics, North Carolina State University, Raleigh, North Carolina 27695, USA*

(Received 18 October 2020; revised 18 October 2021; accepted 2 November 2021; published 18 November 2021)

Time-resolved measurements provide a new way to disentangle complex interactions in quantum materials due to their different timescales. We used pump-probe Raman scattering to investigate the apical oxygen vibration in $YBa_2Cu_3O_{6+x}$ under nonequilibrium conditions. Time dependence of the phonon population demonstrated strong electron-phonon coupling. Most importantly, the phonon shifts to a higher energy due to transient smearing of the Fermi surface in a remarkable agreement with diagrammatic theory. We also discuss insights into photoinduced superconductivity reported at lower doping that follow from these results.

DOI: 10.1103/PhysRevB.104.L180505

Driving quantum materials with electromagnetic fields can generate novel phases and states away from thermal equilibrium [1–5]. Recently reported signatures of superconductivity at elevated temperatures in photoexcited copper oxides and intercalated fullerenes are particularly interesting but still enigmatic [6–12]. In most of these experiments the ultrafast laser pulse (pump) drives or photoexcites the system and another ultrafast pulse (probe) takes snapshots of a specific property as a function of pump-probe time delay. Such experiments also elucidate energy flows between phonons, electrons, and magnons providing a way to determine the strength of different interactions.

This work focuses on relaxation timescales and interactions between electrons and phonons in a prototypical copper oxide superconductor, $YBa_2Cu_3O_{6+x}$.

Electron-phonon coupling in the copper oxides is still enigmatic. It allows electron-hole recombination and electron scattering with the creation or annihilation of phonons; phonons in turn can decay into electron-hole pairs. As a result, spectroscopic quasiparticle peaks shift and/or broaden due to decreased lifetime. However, electron-phonon scattering is not the only process that gives rise to these effects. Internally, phonon-phonon coupling (anharmonicity) also broadens the phonon peaks; similarly, electron-electron interactions can broaden the electronic quasiparticles, as does disorder [13]. Thus, extracting just the electron-phonon coupling strength from the linewidths of quasiparticle peaks is challenging.

To get around this problem, we used time-resolved Raman scattering (TRR) [Fig. 1(a)] [14–23]. In TRR an ultrafast optical pump laser pulse first photoexcites the material and Raman scattering from another time-delayed pulse probes the system. In the copper oxides, previous TRR work highlighted ultrafast destruction of the antiferromagnetic order in the undoped parent compound of $YBa_2Cu_3O_{6+x}$ [24] and nonequilibrium behavior of the superconducting gap in $Bi_2Sr_2CaCu_2O_{8+\delta}$ (BSCCO) [25].

In our experiment near-infrared (IR) pump pulses create hot electrons, and the time-delayed Raman probe measures the apical oxygen A_{1g} phonon. Apical oxygen modes recently came to the center of attention due to their impact on electronic [26] and magnetic [27] degrees of freedom of the copper-oxygen planes, interlayer charge transport [28], and photoinduced superconductivity [6,9–11,26]. The A_{1g} mode is known for a large spectroscopic linewidth [29–31] and an anomaly at the superconducting transition temperature, T_c.

Upon optical pumping the phonon occupation number increased dramatically due to absorption of energy from photoexcited electrons as expected from strong electron-phonon coupling [32–37]. This phonon also hardened at short time delays as a result of the decrease of its electronic self-energy expected from smearing of the Fermi surface due to very high transient electronic temperature. This effect provides a rigorous test of electron-phonon calculations based on electronic structure. Our results were in quantitative agreement with the Green's functions–based theory of Refs. [33,38] [see Fig. 1(b)].

Data presented in this Letter were collected on a 170-nm-thick (110)-oriented $YBa_2Cu_3O_{6.9}$ thin film prepared by pulsed laser deposition on a (110) $LaAlO_3$ substrate with T_c of 81 K [39,40]. We also obtained a data set on a similar film with reduced oxygen concentration ($T_c = 40$ K) with the temperature in the cryostat of 100 K. Our TRR setup [Fig. 1(a)] uses 20-kHz 790-nm (1.57 eV) laser pulses from an amplified mode-locked Ti:sapphire laser, which produces intense 40 fs pulses. Second-harmonic generation at 395 nm (3.14 eV) was used as the probe light source for Raman scattering.

*Corresponding author: dmitry.reznik@colorado.edu

 ©2021 American Physical Society

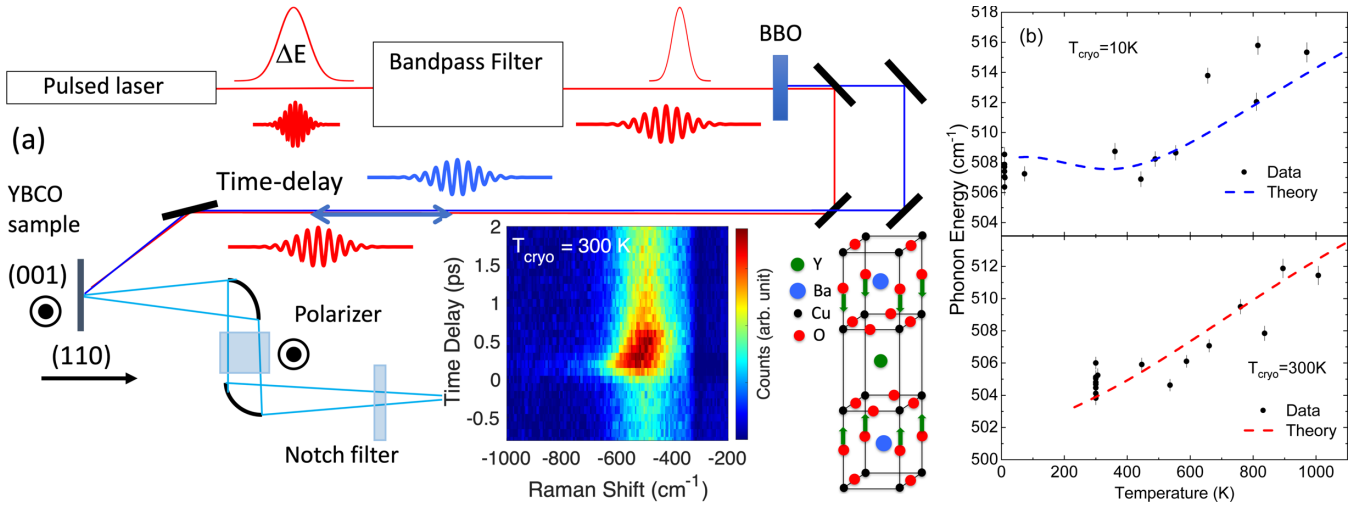

FIG. 1. Time-resolved Raman scattering (TRR) setup and key results. (a) Schematic of the TRR experiment and the color map showing representative data on the anti-Stokes (AS) side of the spectrum obtained with the sample at 300 K. Negative time corresponds to the probe pulse arriving before the pump pulse when the system is still at thermal equilibrium. Most intensity in the peak is from the apical oxygen phonon whose atomic displacements are indicated by green arrows in the schematic of the $YBa_2Cu_3O_7$ unit cell to the right of the color map. (b) Comparison of diagrammatic theory [38] and experiment for the dependence of phonon energy as a function of electronic temperature at delay times up to 600 fs. The temperature in the cryostat was 10 K/300 K in the top/bottom panels, respectively. Impurity scattering of 20 meV was added to the theory curve in the upper panel, but not to the lower panel, since scattering by phonons at 300 K is greater. Unrenormalized phonon energy was picked to obtain good agreement of theory with experiment at thermal equilibrium [38].

The time-energy uncertainty principle limits the energy resolution of the ultrafast probe. In order to resolve the phonons from the elastic line, the 790 nm pulses were passed through an in-house-built time-compensating band-pass filter [Fig. 1(a)] making both the pump and the probe pulses narrower in energy and broader in time. A cross-correlation measurement gave a time resolution of 220 fs FWHM (see Supplementary Note 1 in [41]). The time-averaged probe power was below 1 mW, to eliminate self-pumping nonlinearities (in the Supplemental Material [41], see Ref. [17] therein).

The scattered light was collected by a pair of parabolic mirrors with a polarizer in the middle, and analyzed on a single-stage McPherson spectrometer equipped with a LN_2-cooled CCD detector. A custom-made notch filter blocked elastically scattered light. The samples were in air or in a cryostat in a He exchange gas. We show results obtained with the pump photon polarization parallel to the *ab* plane. Photon polarization along the *c* axis gave similar results. Background measured under identical conditions but without the probe was subtracted from raw data.

We read off phonon temperature from the intensities on the Stokes (S) and anti-Stokes (AS) sides, I_S and I_{AS} [15,16]. They are related by the fundamental principle of detailed balance:

$$\frac{gI_{AS}}{I_S} = \frac{(\omega_0 + \omega_{ph})^4}{(\omega_0 - \omega_{ph})^4} e^{-\hbar\omega_{ph}/k_B T_{ph}}, \quad (1)$$

where ω_0 is the laser frequency, ω_{ph} is the phonon energy, k_B is the Boltzmann constant, T_{ph} is the phonon temperature, and g is equal to 1. Introducing g allows us to correct for the systematic error due to imprecise spectrometer calibration. We made $g = 0.9$ to make the phonon temperature at negative times equal to 300 K at room temperature. Following convention, we define the temperature of each bosonic mode, T_{boson}, via its relation to the occupation number $n = (e^{\hbar\omega_{ph}/k_B T_{\text{boson}}} - 1)^{-1}$. Away from thermal equilibrium different phonons have different occupation numbers, and therefore different temperatures. According to the fluctuation-dissipation theorem, the S and AS Raman intensities are given by $I_S = (n+1)\chi''(\hbar\omega)$ and $I_{AS} = n\chi''(\hbar\omega)$, where χ'' is the imaginary part of the Raman response function (polarizability) of the phonon of interest. The color map in Fig. 1(a) showcases the dramatic increase of the AS intensity, indicating an increase of T_{ph} [Eqs. (1), (2)], as well as a peak shift to larger energy right after photoexcitation.

The apical oxygen phonon around 500 cm^{-1} and a weaker plane oxygen mode at 440 cm^{-1} [Fig. 2(a), inset], which may include substantial apical oxygen character [42,43], dominate the Raman spectrum in the *zz* geometry where both incident and scattered photons are polarized perpendicular to the copper-oxygen planes [Fig. 2(a)] [29,30,44]. The intrinsic line shape of the phonon peaks is known to be best described by characteristic Fano profiles (see inset in Fig. 2(a) and [29,30,44]); however, due to a very broad energy resolution of the experiment, they were fitted with Gaussians as shown in the main panel of Fig. 2(a). When fitting the time-resolved data where the peaks are not resolved [Fig. 2(a), main panel], the intensity of the 440 cm^{-1} peak was fixed at 20% of the 500 cm^{-1} peak, consistent with Raman intensities obtained with a high-energy-resolution 360 nm laser whose wavelength is close to 395 nm of the probe pulsed laser. The linewidths of the two peaks are similar [Fig. 2(a), inset], so we assumed similar electron-phonon coupling and kept the intensity ratio the same at all delay times. Assuming weak electron-phonon coupling for the 440 cm^{-1} peak did not significantly change the fit results.

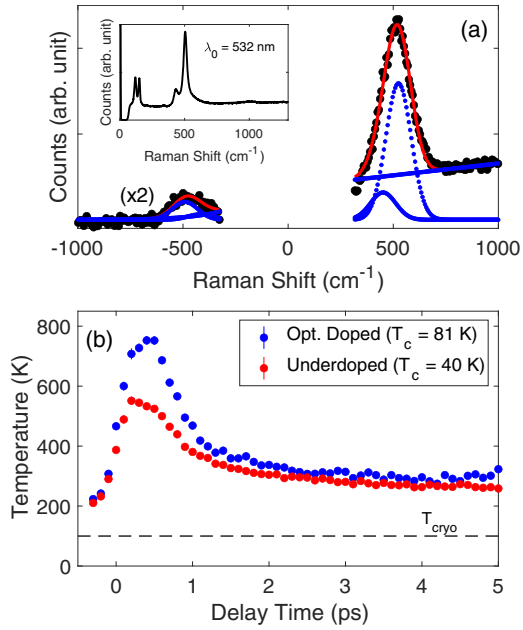

FIG. 2. Raw data and phonon temperature at two doping levels. (a) Background-subtracted TRR spectra at different delay times with the cryostat at 300 K (black circles). The peaks at ± 500 cm^{-1} are Stokes (+) and anti-Stokes (−) phonon peaks. Red line is a guide to the eye representing smoothed data without the pump. Large peak widths are due to the increased energy width of the pulsed laser. (b) Phonon temperature as a function of time after photoexcitation at optimal doping and reduced doping where photoinduced superconductivity was reported earlier [9]. Temperature in the cryostat of 100 K and pump fluence of 8 mJ/cm^2 were the same as in Ref. [9]. Note that pump energy is absorbed first by electron-hole pairs, which then thermalize with the apical oxygen phonons; i.e., electronic temperature never drops below the phonon temperatures.

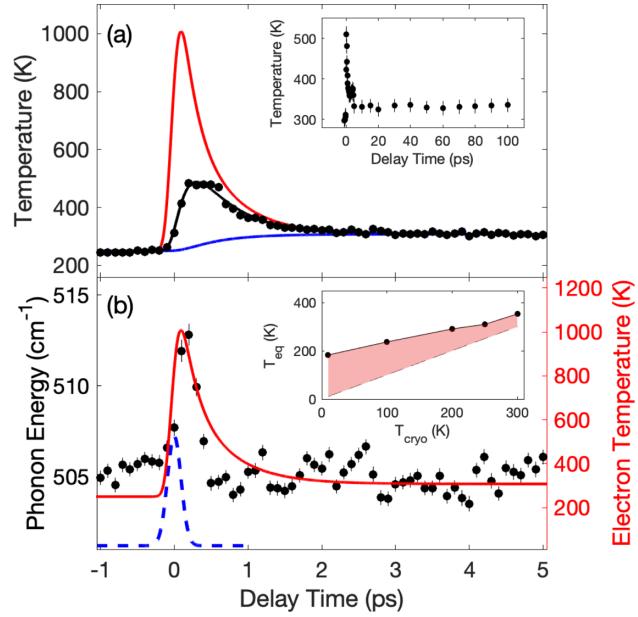

FIG. 3. Phonon temperature and energy together with fits to the two-temperature model. Pump (probe) fluence was 1.4 mJ/cm^2 (15 μJ/cm^2). $T_{\rm cryo}$ was 250 K. Black line represents hot phonons; red, hot electrons; blue, cold phonons. The electronic temperature curves in (a) and (b) are the same. Inset to (a) illustrates the behavior at large delay times for the sample in air at 300 K. Dashed blue line in (b) is the measured pump-probe cross correlation centered at $t = 0$.

Figure 2(b) shows the time dependence of the phonon temperature for optimally doped and underdoped samples obtained under the pumping conditions used to generate transient superconductivity with the near-IR pump in an earlier study [9]. The two samples behave similarly with smaller maximum temperature achieved by the underdoped sample. Note that in both cases the phonon temperature remains above 300 K up to long delay times although the temperature in the cryostat was 100 K.

We performed a detailed analysis of the time-dependent phonon data obtained with a lower pump fluence (Fig. 3). The phonon temperature dramatically increases within the time resolution to about 450 K independently of the temperature in the cryostat. This increase is followed by the exponential decay starting from 0.5 ps. The decay saturates around 5 ps [Fig. 3(a), inset] when the photoexcited region reaches the internal thermal equilibrium temperature, $T_{\rm eq} = 300$ K. The inset to Fig. 3(b) shows $T_{\rm eq}$ as a function of $T_{\rm cryo}$ highlighting increased transient heating of the sample, ΔT, at lower temperatures due to its smaller heat capacity. Further equilibration with the cryostat exchange gas is much longer than 100 ps [see inset to Fig. 3(a)]. An earlier study attributed this heating to nonthermal effects, but the heating at these time delays is consistent with the pump fluence as discussed below.

Our 1.5 eV pump photons should create electron-hole pairs [45], which thermalize among themselves much faster than the time resolution. Time-resolved angle-resolved photoemission (trARPES) showed that electrons reached a maximum temperature of 800 K with 100 μJ/cm^2 pump pulses in BSCCO [46]. In graphite the electronic temperature reached far above 1000 K when pumping with 150 μJ/cm^2 [15,47,48]. It is reasonable to expect similarly high electronic temperatures in YBCO.

We interpret our results in terms of the two-temperature model where f is a fraction of phonons with strong electron-phonon coupling, λ. Photoexcited electrons first give off energy to the hot phonons [46,49,50], which in turn decay into other, cold phonons with the lifetime τ until all phonons and electrons thermalize at $T_{\rm eq}$. The system then slowly equilibrates with the heat bath via propagating (mostly acoustic) phonons.

Our experiments provide detailed information on each step of this process.

The electrons are pumped by a Gaussian pulse $P(t)$ with energy density $E_{\rm pulse} = c_{\rm tot}\Delta T$, where $\Delta T = T_{\rm eq} - T_{\rm cryo}$ and the duration is 170 fs. The combined specific heat of electrons, hot phonons, and cold phonons, $c_{\rm tot}$, depends on temperature, but we approximate it as the average of the values at $T_{\rm cryo}$ and $T_{\rm eq}$ taken from Ref. [51]. If Ω_0 is a typical phonon energy, then the electronic temperature, T_{el}, the hot phonon temperature, T_h, and the cold phonon temperature, T_c, obey the rate

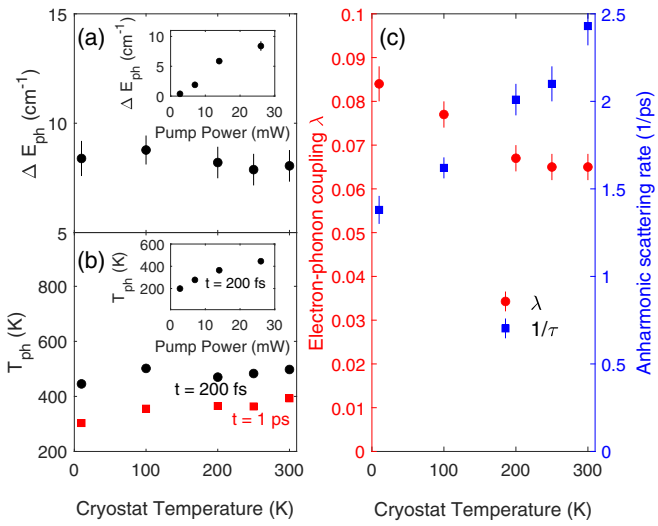

FIG. 4. Dependence on pump power, P, and $T_{\rm cryo}$. (a) Phonon hardening at 200 fs $[E_{ph}(200\ \text{fs}) - E_{ph}(-1000\ \text{fs})]$ as a function of $T_{\rm cryo}$ at $P = 27$ mW. Inset: Phonon hardening at $T_{\rm cryo} = 10$ K as a function of P. (b) Phonon temperature at 200 fs and 1 ps as a function of $T_{\rm cryo}$ at $P = 27$ mW (fluence of 1.4 mJ/cm^2). Note that $T_{el} = T_{ph}$ at 1 ps. Inset: T_{ph} at 200 fs at $T_{\rm cryo} = 10$ K as a function of P. (c) Electron-phonon coupling constant λ together with the anharmonic scattering rate $1/\tau$. See Supplementary Notes 2 and 3 for details on how τ and λ were calculated [41]

equations:

$$\frac{\partial T_{el}}{\partial t} = -\frac{3\lambda\Omega_0^3}{\hbar\pi k_B^2}\frac{n(T_{el}) - n(T_h)}{T_{el}} + \frac{P(t)}{c_{el}(T_{el})}, \tag{2}$$

$$\frac{\partial T_h}{\partial t} = \frac{c_{el}(T_{el})}{c_h(T_h)}\frac{3\lambda\Omega_0^3}{\hbar\pi k_B^2}\frac{n(T_{el}) - n(T_h)}{T_{el}} - \frac{T_h - T_c}{\tau}, \tag{3}$$

$$\frac{\partial T_c}{\partial t} = \frac{c_h(T_h)}{c_c(T_c)}\frac{T_h - T_c}{\tau}, \tag{4}$$

where $n(T) = (e^{\Omega_0/k_BT} - 1)^{-1}$ and the specific heats are $c_{el} = \gamma T_{el}$, $c_h = 3N_{\rm atm} f\Omega_0(\partial n_h/\partial T_h)$, and $c_c = 3N_{\rm atm}(1 - f)\Omega_0(\partial n_c/\partial T_c)$. Here, $N_{\rm atm}$ is the number of atoms per formula unit (= 12.9 for our sample) and the value of γ was taken from measurements in Ref. [51]. Equations (2)–(4) correspond to Eqs. (1)–(3) of Ref. [46] written down in terms of ΔT, which we measured with high precision.

We solved these coupled differential equations using the Euler method with 1 fs steps. Figure 3(a) presents a fit to this model with $\Omega_0 = 60$ meV and $\tau = 478 \pm 25$ fs (see Supplementary Note 3 for fits with different values of Ω_0 and τ [41]). $f = 0.14$ and $\lambda = 0.065$ were free parameters. Electrons initially heat up to 1000 K similarly to the previous result on BSCCO [46], and then cool quickly to thermalize with hot phonons at 300 fs. Thermalized hot electrons and hot phonons have a larger heat capacity compared with the heat capacity of electrons alone so they equilibrate with cold phonons with the much slower 478 fs time constant at 250 K. This lifetime increases with reduced temperature reaching 700 fs at 10 K (see Fig. 4(c) and Supplementary Note 2 in [41]). It is much smaller than in graphite [15–21]. The electron-phonon coupling strength is close to $\lambda = 0.07$ at all temperatures, which is smaller than the the LDA value [52].

Thermalization on subpicosecond timescales is controversial. Deviations from the Fermi-Dirac distributions of the electrons have been reported at pump-probe delay times of a few hundred fs in simple metals [53,54]. However, the ARPES measurements of Ref. [40] showed that in BSCCO, thermalization occurs already at 100 fs. It also showed that nonthermal distribution at shorter times is characterized by a small (only a few percent) deviation from the Fermi-Dirac distribution. Assuming that YBCO behaves similarly, for our purposes electrons can be treated as internally thermalized [53].

The assumption of internally thermalized hot phonons is valid only if they have similar electron-phonon coupling strength. For example, the 2T model breaks down in graphite where one hot phonon had a significantly larger electron-phonon coupling than another [15]. According to Ref. [33] as well as prior experimental work, the breathing phonons and the buckling phonons have a significantly stronger electron-phonon coupling than the apical oxygen mode [55,56]. We found that adding phonons that have a much stronger electron-phonon coupling than the apical mode to the model can increase λ by nearly an order of magnitude; thus λ obtained from fits to the apical oxygen phonon occupation data alone is not accurate. Time-dependent electronic temperature, however, was only weakly model dependent, which allowed us to make a quantitative comparison of the phonon energy vs electronic temperature to theory as discussed below.

We observe a profound shift of the phonon peak position to a higher energy (hardening) at small time delays [Fig. 3(b)] with the maximum at 200 fs. It is independent of $T_{\rm cryo}$ but decreases with reduced pump power [Fig. 4(a)]. These changes in the phonon energy do not correlate with either phonon occupation or with the electric field of the pump, which should follow the cross-correlation curve in Fig. 3(c). Instead phonon hardening closely follows the electronic temperature. A similar effect in graphite was associated with electronic temperatures of over 1000 K [17,57,58].

The phonon self-energy $\Pi(q, \Omega)$ is proportional to electronic polarizability, which depends on the electronic temperature [59–61]. To make this quantitative, we model the system as a band of electrons interacting with the three strongly coupled phonons: the A_{1g}, B_{1g}, and breathing modes, which are kept at the cryostat temperature. Electronic quasiparticle excitations renormalize the apical phonon frequency. The increase in the quasiparticle temperature diminishes the softening of the apical phonon [lines in Fig. 1(b)], leading to an increase in the phonon frequency as a function of the effective electronic temperature [60] (also see Supplementary Note 4 in [41] and Refs. [33,62] therein for the details). The initial decrease of the theory curve at $T_{\rm cryo} = 10$ K is a result of the broadening of the electronic bands due to their phonon-mediated self-energy. At weak interactions (and low T) broadening the bands increases the bubble (phonon self-energy), and thus softens the phonon as temperature increases. This effect competes with the dominant hardening effect due to smearing of the Fermi surface described above. The calculation picks it up due to relatively sharp bands when the lattice temperature is low in the absence of impurity scattering. It is not present at 300 K because of the existing broadening by phonons at this

temperature. Increasing the impurity scattering rate weakens the kink at $T_{cryo} = 10$ K as shown in Supplementary Note 5 [41].

Note that simple heating of the sample leads to phonon softening, not hardening. This is primarily because of thermal expansion caused by increased population of acoustic phonons. However, acoustic phonons stay cold at short pump-probe time delays and lattice expansion does not occur.

We have demonstrated quantitative agreement with theory of the time-varying apical phonon frequency as the electronic system loses its excess energy to the broader phonon bath. It highlights that the dynamics of energy transfer are responsible for the temporal behavior of the electrons and phonons, as well as the disparity between interactions in and out of equilibrium. Although in strongly correlated materials such as YBCO there are strong Coulomb processes and impurity scattering that dominate the electronic spectra, when it comes to time domain these processes rapidly come to an internal equilibrium and effectively shut off [38]. Our results provide a phonon-centered perspective on previous experiment in $Bi_2Sr_2CaCu_2O_8$ with both time-resolved ARPES [63] and ultrafast electron diffraction [64] that both observed a similar quantitative agreement.

Our work provides insights into photoinduced superconductivity [65,66]. Its signatures were recently reported in the optical spectra of underdoped YBCO up to time delays of about 1 ps when pumping with 790-nm near-IR pulses [9] as well as with pulses that resonated with IR-active apical oxygen phonons. Our experiments reproduced the former pumping condition and showed that optimally doped and underdoped YBCO behave similarly [Fig. 2(b)]. We found that hot and cold phonons were out of thermal equilibrium, but electrons and hot phonons were at or near thermal equilibrium at time delays below 1 ps. At these time delays electronic temperatures were always well above room temperature. We plan to determine transient heating while pumping the IR-active phonons in future experiments.

We would like to thank A. Cavalleri for a critical reading of the manuscript and helpful suggestions. Experiments at the University of Colorado were supported by the NSF under Grant No. DMR-1709946, and a laboratory upgrade that made these experiments possible by DARPA through the DRINQS program. The work at University of Wisconsin–Madison (thin-film synthesis and structural and electrical characterizations) was supported by the U.S. Department of Energy (DOE), Office of Science, Office of Basic Energy Sciences (BES), under Award No. DE-FG02-06ER46327. A.F.K. acknowledges support from the National Science Foundation under Grant No. DMR-1752713. The work at the University of Wisconsin–Parkside was supported by WiSys and UW System Applied Research Grant (ARG) Award for 2019-2020 (102-4-812000-AAH1775).

[1] Y. H. Wang, H. Steinberg, P. Jarillo-Herrero, and N. Gedik, Observation of Floquet-Bloch states on the surface of a topological insulator, Science **342**, 453 (2013).

[2] A. Kirilyuk, A. V. Kimel, and T. Rasing, Ultrafast optical manipulation of magnetic order, Rev. Mod. Phys. **82**, 2731 (2010).

[3] P. Tengdin, W. You, C. Chen, X. Shi, D. Zusin, Y. Zhang, C. Gentry, A. Blonsky, M. Keller, P. M. Oppeneer *et al.*, Critical behavior within 20 fs drives the out-of-equilibrium laser-induced magnetic phase transition in nickel, Sci. Adv. **4**, 9744 (2018).

[4] H. Okamoto, T. Miyagoe, K. Kobayashi, H. Uemura, H. Nishioka, H. Matsuzaki, A. Sawa, and Y. Tokura, Photoinduced transition from Mott insulator to metal in the undoped cuprates Nd_2CuO_4 and La_2CuO_4, Phys. Rev. B **83**, 125102 (2011).

[5] H. Ehrke, R. I. Tobey, S. Wall, S. A. Cavill, M. Först, V. Khanna, Th. Garl, N. Stojanovic, D. Prabhakaran, A. T. Boothroyd *et al.*, Photoinduced Melting of Antiferromagnetic Order in $La_{0.5}Sr_{1.5}MnO_4$ Measured Using Ultrafast Resonant Soft X-Ray Diffraction, Phys. Rev. Lett. **106**, 217401 (2011).

[6] W. Hu, S. Kaiser, D. Nicoletti, C. R. Hunt, I. Gierz, M. C. Hoffmann, M. Le Tacon, T. Loew, B. Keimer, and A. Cavalleri, Optically enhanced coherent transport in $YBa_2Cu_3O_{6.5}$ by ultrafast redistribution of interlayer coupling, Nat. Mater. **13**, 705 (2014).

[7] M. Mitrano, A. Cantaluppi, D. Nicoletti, S. Kaiser, A. Perucchi, S. Lupi, P. Di Pietro, D. Pontiroli, M. Riccò, S. R. Clark, D. Jaksch, and A. Cavalleri, Possible light-induced superconductivity in K_3C_{60} at high temperature, Nature (London) **530**, 461 (2016).

[8] M. Budden, T. Gebert, M. Buzzi, G. Jotzu, E. Wang, T. Matsuyama, G. Meier, Y. Laplace, D. Pontiroli, M. Riccó, F. Schlawin, D. Jaksch, and A. Cavalleri, Evidence for metastable photo-induced superconductivity in K_3C_{60}, Nat. Phys. **17**, 611 (2021).

[9] B. Liu, M. Först, M. Fechner, D. Nicoletti, J. Porras, T. Loew, B. Keimer, and A. Cavalleri, Pump Frequency Resonances for Light-Induced Incipient Superconductivity in $YBa_2Cu_3O_{6.5}$, Phys. Rev. X **10**, 011053 (2020).

[10] D. Nicoletti, E. Casandruc, Y. Laplace, V. Khanna, C. R. Hunt, S. Kaiser, S. S. Dhesi, G. D. Gu, J. P. Hill, and A. Cavalleri, Optically induced superconductivity in striped $La_{2-x}Ba_xCuO_4$ by polarization-selective excitation in the near infrared, Phys. Rev. B **90**, 100503(R) (2014).

[11] K. A. Cremin, J. Zhang, C. C. Homes, G. D. Gu, Z. Sun, M. M. Fogler, A. J. Millis, D. N. Basov, and R. D. Averitt, Photoenhanced metastable *c*-axis electrodynamics in stripe-ordered cuprate $La_{1.885}Ba_{0.115}CuO_4$, Proc. Natl. Acad. Sci. USA **116**, 19875 (2019).

[12] Y. Takabayashi and K. Prassides, Unconventional high-T_c superconductivity in fullerides, Philos. Trans. Roy. Soc. A **374**, 20150320 (2016).

[13] S. R. Park, A. Hamann, L. Pintschovius, D. Lamago, G. Khaliullin, M. Fujita, K. Yamada, G. D. Gu, J. M. Tranquada, and D. Reznik, Effects of charge inhomogeneities on elementary excitations in $La_{2-x}Sr_xCuO_4$, Phys. Rev. B **84**, 214516 (2011).

[14] D. von der Linde, J. Kuhl, and H. Klingenberg, Raman Scattering from Nonequilibrium LO Phonons with Picosecond Resolution, Phys. Rev. Lett. **44**, 1505 (1980).

[15] J.-A. Yang, S. Parham, D. Dessau, and D. Reznik, Novel electron-phonon relaxation pathway in graphite revealed by time-resolved Raman scattering and angle-resolved photoemission spectroscopy, Sci. Rep. **7**, 40876 (2017).

[16] J. A. Kash, J. C. Tsang, and J. M. Hvam, Subpicosecond Time-Resolved Raman Spectroscopy of LO Phonons in GaAs, Phys. Rev. Lett. **54**, 2151 (1985).

[17] H. Yan, D. Song, K. F. Mak, I. Chatzakis, J. Maultzsch, and T. F. Heinz, Time-resolved Raman spectroscopy of optical phonons in graphite: Phonon anharmonic coupling and anomalous stiffening, Phys. Rev. B **80**, 121403(R) (2009).

[18] D. Song, F. Wang, Gordana Dukovic, M. Zheng, E. D. Semke, Louis E. Brus, and Tony F. Heinz, Direct Measurement of the Lifetime of Optical Phonons in Single-Walled Carbon Nanotubes, Phys. Rev. Lett. **100**, 225503 (2008).

[19] K. Kang, T. Ozel, D. G. Cahill, and M. Shim, Optical phonon lifetimes in single-walled carbon nanotubes by time-resolved Raman scattering, Nano Lett. **8**, 4642 (2008).

[20] K. Kang, D. Abdula, D. G. Cahill, and M. Shim, Lifetimes of optical phonons in graphene and graphite by time-resolved incoherent anti-Stokes Raman scattering, Phys. Rev. B **81**, 165405 (2010).

[21] S. Wu, W.-T. Liu, Xiaogan Liang, P. J. Schuck, F. Wang, Y. R. Shen, and M. Salmeron, Hot phonon dynamics in graphene, Nano Lett. **12**, 5495 (2012).

[22] J. Zhu, R. B. Versteeg, P. Padmanabhan, and P. H. M. van Loosdrecht, Dynamical resonance quench and Fano interference in spontaneous Raman scattering from quasiparticle and collective excitations, Phys. Rev. B **99**, 094305 (2019).

[23] R. B. Versteeg, J. Zhu, P. Padmanabhan, C. Boguschewski, R. German, M. Goedecke, P. Becker, and P. H. M. van Loosdrecht, A tunable time-resolved spontaneous Raman spectroscopy setup for probing ultrafast collective excitation and quasiparticle dynamics in quantum materials, Struct. Dyn. **5**, 044301 (2018).

[24] J.-A. Yang, N. Pellatz, T. Wolf, R. Nandkishore, and D. Reznik, Ultrafast magnetic dynamics in insulating $YBa_2Cu_3O_{6.1}$ revealed by time-resolved two-magnon Raman scattering, Nat. Commun. **11**, 2548 (2020).

[25] R. P. Saichu, I. Mahns, A. Goos, S. Binder, P. May, S. G. Singer, B. Schulz, A. Rusydi, J. Unterhinninghofen, D. Manske, P. Guptasarma, M. S. Williamsen, and M. Rübhausen, Two-Component Dynamics of the Order Parameter of High-Temperature $Bi_2Sr_2CaCu_2O_{8+\delta}$ Superconductors Revealed by Time-Resolved Raman Scattering, Phys. Rev. Lett. **102**, 177004 (2009).

[26] B. Rosenstein and B. Ya. Shapiro, Apical oxygen vibrations dominant role in *d*-wave cuprate superconductivity and its interplay with spin fluctuations, J. Phys. Commun. **5**, 055013 (2021).

[27] Y. Y. Peng, G. Dellea, M. Minola, M. Conni, A. Amorese, D. Di Castro, G. M. De Luca, K. Kummer, M. Salluzzo, X. Sun, X. J. Zhou, G. Balestrino, M. Le Tacon, B. Keimer, L. Braicovich, N. B. Brookes, and G. Ghiringhelli, Influence of apical oxygen on the extent of in-plane exchange interaction in cuprate superconductors, Nat. Phys. **13**, 1201 (2017).

[28] M. H. Michael, A. von Hoegen, M. Fechner, M. Först, A. Cavalleri, and E. Demler, Parametric resonance of Josephson plasma waves: A theory for optically amplified interlayer superconductivity in $YBa_2Cu_3O_{6+x}$, Phys. Rev. B **102**, 174505 (2020).

[29] M. F. Limonov, A. I. Rykov, S. Tajima, and A. Yamanaka, Raman scattering in $YBa_2Cu_3O_7$ single crystals: Anisotropy in normal and superconductivity states, Phys. Solid State **40**, 367 (1998).

[30] E. Altendorf, J. Chrzanowski, J. C. Irwin, A. O'Reilly, and W. N. Hardy, Electron-phonon interactions of Raman-active phonons in $YBa_2Cu_3O_{7-y}$, Phys. C (Amsterdam, Neth.) **175**, 47 (1991).

[31] K. F. McCarty, H. B. Radousky, J. Z. Liu, and R. N. Shelton, Temperature dependence of the linewidths of the Raman-active phonons of $YBa_2Cu_3O_7$: Evidence for a superconducting gap between 440 and 500 cm^{-1}, Phys. Rev. B **43**, 13751 (1991).

[32] O. Gunnarsson and O. Rösch, Interplay between electron-phonon and Coulomb interactions in cuprates, J. Phys.: Condens. Matter **20**, 043201 (2008).

[33] S. Johnston, F. Vernay, B. Moritz, Z.-X. Shen, N. Nagaosa, J. Zaanen, and T. P. Devereaux, Systematic study of electron-phonon coupling to oxygen modes across the cuprates, Phys. Rev. B **82**, 064513 (2010).

[34] A. S. Alexandrov and P. E. Kornilovitch, High-temperature superconductivity and charge segregation in a model with strong long-range electron-phonon and Coulomb interactions, Phys. Lett. A **299**, 650 (2002).

[35] C. Falter, Michael Klenner, and Georg A. Hoffmann, Phonon renormalization and *c*-axis phonon-plasmon mixing in La_2CuO_4, Phys. Rev. B **52**, 3702 (1995).

[36] C. Falter, M. Klenner, and W. Ludwig, Effect of charge fluctuations on the phonon dispersion and electron-phonon interaction in La_2CuO_4, Phys. Rev. B **47**, 5390 (1993).

[37] O. Rösch, O. Gunnarsson, X. J. Zhou, T. Yoshida, T. Sasagawa, A. Fujimori, Z. Hussain, Z.-X. Shen, and S. Uchida, Polaronic Behavior of Undoped High-T_c Cuprate Superconductors from Angle-Resolved Photoemission Spectra, Phys. Rev. Lett. **95**, 227002 (2005).

[38] A. F. Kemper, O. Abdurazakov, and J. K. Freericks, General Principles for the Nonequilibrium Relaxation of Populations in Quantum Materials, Phys. Rev. X **8**, 041009 (2018).

[39] J. Z. Wu, P. Y. Hsieh, A. V. McGuire, D. L. Schmidt, L. T. Wood, Y. Shen, and W. K. Chu, Anisotropic properties of the high-quality epitaxial $YBa_2Cu_3O_{7-\delta}(110)$ thin film, Phys. Rev. B **44**, 12643 (1991).

[40] M. S. Raven, E. E. Inameti, S. Iwama, Y. M. Wan, and B. G. Murray, Epitaxial growth and critical currents in (013)/(103)- and (110)-oriented $YBa_2Cu_3O_x$ films, Phys. Rev. B **52**, 6845 (1995).

[41] See Supplemental Material at http://link.aps.org/supplemental/10.1103/PhysRevB.104.L180505 for more information on experimental, calculation and fitting details.

[42] C. Ambrosch-Draxl, H. Auer, R. Kouba, E. Ya. Sherman, P. Knoll, and M. Mayer, Raman scattering in $YBa_2Cu_3O_7$: A comprehensive theoretical study in comparison with experiments, Phys. Rev. B **65**, 064501 (2002).

[43] O. V. Misochko, E. I. Rashba, E. Ya. Sherman, and V. B Timofeev, On the mixing of vibrational modes in high-T_c superconductors, Phys. Rep. **194**, 387 (1990).

[44] D. Reznik, M. V. Klein, W. C. Lee, D. M. Ginsberg, and S-W. Cheong, Effect of conduction electrons on the polarized Raman spectra of copper oxide superconductors, Phys. Rev. B **46**, 11725 (1992).

[45] S. L. Cooper, D. Reznik, A. Kotz, M. A. Karlow, R. Liu, M. V. Klein, W. C. Lee, J. Giapintzakis, D. M. Ginsberg, B. W. Veal, and A. P. Paulikas, Optical studies of the *a*-, *b*-, and *c*-axis charge dynamics in $YBa_2Cu_3O_{6+x}$, Phys. Rev. B **47**, 8233 (1993).

[46] L. Perfetti, P. A. Loukakos, M. Lisowski, U. Bovensiepen, H. Eisaki, and M. Wolf, Ultrafast Electron Relaxation in Superconducting $Bi_2Sr_2CaCu_2O_{8+\delta}$ by Time-Resolved Photoelectron Spectroscopy, Phys. Rev. Lett. **99**, 197001 (2007).

[47] Y. Ishida, T. Togashi, K. Yamamoto, M. Tanaka, T. Taniuchi, T. Kiss, M. Nakajima, T. Suemoto, and S. Shin, Non-thermal hot electrons ultrafastly generating hot optical phonons in graphite, Sci. Rep. **1**, 64 (2011).

[48] M. Breusing, C. Ropers, and T. Elsaesser, Ultrafast Carrier Dynamics in Graphite, Phys. Rev. Lett. **102**, 086809 (2009).

[49] J. C. Johannsen, S. Ulstrup, F. Cilento, A. Crepaldi, M. Zacchigna, C. Cacho, I. C. Edmond Turco, E. Springate, F. Fromm, C. Raidel, T. Seyller, F. Parmigiani, M. Grioni, and P. Hofmann, Direct View of Hot Carrier Dynamics in Graphene, Phys. Rev. Lett. **111**, 027403 (2013).

[50] T. Kampfrath, L. Perfetti, F. Schapper, C. Frischkorn, and M. Wolf, Strongly Coupled Optical Phonons in the Ultrafast Dynamics of the Electronic Energy and Current Relaxation in Graphite, Phys. Rev. Lett. **95**, 187403 (2005).

[51] J. W. Loram, K. A. Mirza, J. R. Cooper, and W. Y. Liang, Electronic Specific Heat of $YBa_2Cu_3O_{6+x}$ from 1.8 to 300 K, Phys. Rev. Lett. **71**, 1740 (1993).

[52] K.-P. Bohnen, R. Heid, and M. Krauss, Phonon dispersion and electron-phonon interaction for $YBa_2Cu_3O_7$ from first-principles calculations, Europhys. Lett. **64**, 104 (2003).

[53] W. S. Fann, R. Storz, H. W. K. Tom, and J. Bokor, Direct Measurement of Nonequilibrium Electron-Energy Distributions in Subpicosecond Laser-Heated Gold Films, Phys. Rev. Lett. **68**, 2834 (1992).

[54] U. Ritzmann, P. M. Oppeneer, and P. Maldonado, Theory of out-of-equilibrium electron and phonon dynamics in metals after femtosecond laser excitation, Phys. Rev. B **102**, 214305 (2020).

[55] D. Reznik, Phonon anomalies and dynamic stripes, Phys. C (Amsterdam, Neth.) **481**, 75 (2012).

[56] M. Raichle, D. Reznik, D. Lamago, R. Heid, Y. Li, M. Bakr, C. Ulrich, V. Hinkov, K. Hradil, C. T. Lin, and B. Keimer, Highly Anisotropic Anomaly in the Dispersion of the Copper-Oxygen Bond-Bending Phonon in Superconducting $YBa_2Cu_3O_7$ from Inelastic Neutron Scattering, Phys. Rev. Lett. **107**, 177004 (2011).

[57] E. A. A. Pogna, S. D. Conte, G. Soavi, V. G. Kravets, Y.-J. Kim, S. Longhi, A. N. Grigorenko, G. Cerullo, and G. D. Valle, Ultrafast spectroscopy of graphene-protected thin copper films, ACS Photon. **3**, 1508 (2016).

[58] M. Obergfell and J. Demsar, Tracking the Time Evolution of the Electron Distribution Function in Copper by Femtosecond Broadband Optical Spectroscopy, Phys. Rev. Lett. **124**, 037401 (2020).

[59] D. Lamago, M. Hoesch, M. Krisch, R. Heid, K.-P. Bohnen, P. Böni, and D. Reznik, Measurement of strong phonon softening in Cr with and without Fermi-surface nesting by inelastic x-ray scattering, Phys. Rev. B **82**, 195121 (2010).

[60] O. Abdurazakov, D. Nevola, A. Rustagi, J. K. Freericks, D. B. Dougherty, and A. F. Kemper, Nonequilibrium electron dynamics in pump-probe spectroscopy: Role of excited phonon populations, Phys. Rev. B **98**, 245110 (2018).

[61] G. Coslovich, B. Huber, W.-S. Lee, Y.-D. Chuang, Y. Zhu, T. Sasagawa, Z. Hussain, H. A. Bechtel, M. C. Martin, Z.-X. Shen, R. W. Schoenlein, and R. A. Kaindl, Ultrafast charge localization in a stripe-phase nickelate, Nat. Commun. **4**, 2643 (2013).

[62] M. R. Norman, Linear response theory and the universal nature of the magnetic excitation spectrum of the cuprates, Phys. Rev. B **75**, 184514 (2007).

[63] J. D. Rameau, S. Freutel, A. F. Kemper, M. A. Sentef, J. K. Freericks, I. Avigo, M. Ligges, L. Rettig, Y. Yoshida, H. Eisaki *et al.*, Energy dissipation from a correlated system driven out of equilibrium, Nat. Commun. **7**, 13761 (2016).

[64] T. Konstantinova, J. D. Rameau, A. H. Reid, O. Abdurazakov, L. Wu, R. Li, X. Shen, G. Gu, Y. Huang, L. Rettig *et al.*, Nonequilibrium electron and lattice dynamics of strongly correlated $Bi_2Sr_2CaCu_2O_{8+\delta}$ single crystals, Sci. Adv. **4**, eaap7427 (2018).

[65] C. R. Hunt, D. Nicoletti, S. Kaiser, D. Pröpper, T. Loew, J. Porras, B. Keimer, and A. Cavalleri, Dynamical decoherence of the light-induced interlayer coupling in $YBa_2Cu_3O_{6+\delta}$, Phys. Rev. B **94**, 224303 (2016).

[66] S. Kaiser, C. R. Hunt, D. Nicoletti, W. Hu, I. Gierz, H. Y. Liu, M. Le Tacon, T. Loew, D. Haug, B. Keimer, and A. Cavalleri, Optically induced coherent transport far above T_c in underdoped $YBa_2Cu_3O_{6+\delta}$, Phys. Rev. B **89**, 184516 (2014).